RNA-silencing induces target gene relocalization toward a specialized nuage domain

Yuchen Yang[1,], David Grunwald[1,], James R. Priess[2,3] and Craig C. Mello[1,4,5*]

Author Affiliations:

1. RNA Therapeutics Institute, University of Massachusetts Medical School, Worcester, MA 01605
2. Fred Hutchinson Cancer Research Center, Seattle, Washington, United States
3. Department of Biology, University of Washington, Seattle, Washington, United States
4. Program in Molecular Medicine, University of Massachusetts Medical School, 368 Plantation Street, Worcester, MA, 01605 United States
5. Howard Hughes Medical Institute, University of Massachusetts Medical School, Worcester, MA, USA

* Correspondence, Craig.Mello@umassmed.edu.

Argonaute small RNA pathways maintain genome integrity and fertility by enforcing the transgenerational silencing of transposons as well as many developmentally regulated germline genes [1]. To propagate silencing, Argonaute pathways coordinate heterochromatin silencing with cycles of small RNA amplification [2]. In animal germlines, mRNA surveillance is thought to occur within cytoplasmic perinuclear domains called nuage [3]. In *C. elegans* 20-50 nuage droplets called P granules surround each pachytene germline nucleus. P granules are known to host many of the Argonaute small RNA systems that carry out transcriptome surveillance, but what if any specific roles P granules might play in Argonaute silencing have remained mysterious. Here we show that RNAi triggers the expansion of a unique P granule, which accumulates large amounts of the target RNA. As transcriptional silencing ensues, both alleles of the target gene relocate near the inner nuclear membrane (INM) directly adjacent this enlarged P granule. Similarly, during piRNA-mediated silencing, both alleles of a target gene reside adjacent to a P granule containing target RNA sequences. In an Argonaute mutant defective in piRNA silencing, the target RNA is released from nuage, and the target alleles dissociate from each other and from the INM. Our findings suggest that transcriptome-surveillance tasks are sub-divided between nuage domains that become specialized to coordinate small RNA silencing signals to their heterochromatin targets.

In the *C. elegans* germline, two major Argonaute pathways initiated by different mechanisms—the piRNA pathway mediated by the Piwi Argonuate PRG-1 and the

dsRNA-initiated RNAi pathway mediated by the Argonaute RDE-1—rely on a common set of downstream small RNA and chromatin effectors that maintain heritable silencing [4]. Argonaute proteins and the machinery that produces their small RNA cofactors localize to perinuclear nuage, where they are thought to act in mRNA surveillance and in the amplification of small-RNA silencing signals [4]. In the *C. elegans* meiotic germline each perinuclear nuage, or P granule, is localized over a cluster of nuclear pores [5], where it has the potential to intercept nascent mRNA *en route* to the cytoplasm [6]. Although previous cytological studies demonstrated the rapid loss of target mRNA in the cytoplasm during RNAi [6,7], changes in the P granules or associated RNAs were not observed during silencing, and thus the dynamics and spatial relationships between nuage and the mRNA and DNA targets of silencing have remained mysterious.

Recent advances in RNA and DNA FISH technology have greatly enhanced the ability to track molecules at subcellular resolution [8-10]. For example, splinted fluorescent probes that assemble multiple fluorophores at a single target greatly amplify DNA FISH signals and permit detection of single genes [9,10]. We therefore decided to use these improved reagents to revisit the cytological events associated with Argonaute silencing. To visualize the spatial and temporal response to RNAi, we exposed worms to *oma-1* dsRNA and monitored *oma-1* mRNA- and DNA-FISH signals simultaneously over a time course of silencing. To distinguish cytoplasmic and nuclear FISH signals, we marked the outer membrane of the nuclear envelope using a GFP::ZYG-12 fusion protein [11] (Figure 1A-1F). In separate gonads we also imaged GFP::GLH-1, a marker for P granules, Figure 1G-L) [12]. We examined the pachytene region of the gonad, where germ cells are connected to a large, shared region of cytoplasm called the core. As

expected from previous studies, *oma-1* mRNA in untreated animals was present at low levels in P-granules and the surrounding cytoplasm, and was abundant–in the gonad core (Figures 1A, 1D and 1J). In addition, we detected a double dot of *oma-1* RNA inside each germ nucleus throughout the pachytene region (Figure 1D), presumably representing transcription from the *oma-1* genes on the paired homologous chromosomes.

As expected, RNAi induced a rapid, marked depletion of *oma-1* mRNA in the germ cell cytoplasm and in the core cytoplasm (for example, compare Figure 1A to 1B and 1C). In the same gonads, however, an *oma-1* RNA signal appeared to increase within a large, perinuclear focus adjacent to each nucleus (Figure 1E). This perinuclear RNA signal persisted for several hours, ultimately decreasing in size by 21 hours (Figure 1C and 1F).

Prior to RNAi, the perinuclear P granules varied in size (green signal in Figures 1G and 1J). By 6 hours of RNAi, one P granule on each nucleus appeared much larger than neighboring nuage, and colocalized with the prominent, enlarged *oma-1* RNA focus (Figures 1H and 1K). Thus, dsRNA-mediated silencing appears to trigger differentiation between the P granules on the same nucleus, with target RNA accumulating in only one enlarged P granule.

The location of the *oma-1* RNA signal within the nucleus exhibited dramatic changes during RNAi. Whereas prior to RNAi each pachytene nucleus exhibited paired foci of RNA signal, by 6 hours many nuclei exhibited only a single focus of nuclear RNA that was located directly adjacent the INM and the enlarged P granule (Figure 1E and

1K). By 21 hours the proportion of nuclei with this single focus of nuclear RNA had increased to 100% (Figure 1L).

Prompted by these striking changes in nuclear RNA localization we wished to examine whether the *oma-1* DNA undergoes similar changes. Prior to RNAi (at time zero), we detected *oma-1* DNA in two, well-separated foci (double dots) flanking the paired homologous chromosomes, and at variable distances from INM. These paired DNA signals precisely coincided with the aforementioned nuclear RNA signals (Figure 1Ai-iii), and thus are likely to represent the *oma-1* transcription sites. By contrast, a single bright focus (single dot) of *oma-1* DNA signal was detected in ~40% of nuclei (n=31/77) after 6 hours of RNAi and in 100% of nuclei (n>100) after 21 hours (Figure 1B and 1C). These results suggest that RNAi causes the *oma-1* genes on the paired, homologous chromosomes to move close together, such that they can no longer be resolved as separate foci. Notably, in nuclei with the single dot of DNA signal, the DNA was always adjacent to the INM (Figure 1E and 1F), and directly beneath the perinuclear, enlarged P granule and RNA signals (for example, compare inset images in Figures 1H to 1K).

In order to determine whether genes in the RNAi pathway are required for the specialized nuage body, we repeated the above assays in the mutant *rde-3*. The *rde-3* gene encodes an effector of RNAi silencing that is required both in the animals exposed to dsRNA and for inherited silencing among their offspring [13]. We found that *oma-1* dsRNA did not trigger any of the cytological changes in *rde-3* mutants that were observed in wild-type worms: The double dots of *oma-1* DNA did not relocalize toward the INM, low levels of *oma-1* RNA remained on many of the perinuclear P granules,

which appeared similar in size to those in untreated controls, and cytoplasmic *oma-1* mRNA remained abundant in the gonad core (Figure 2A and 2B and Sup Figure 2). Together these results show that RNAi triggers the development of a specialized enlarged nuage body, followed by localization of the target genes to the proximal INM.

RNAi is known to trigger nuclear events including the deposition of repressive chromatin on target loci [14], and several studies have linked heterochromatin formation to the localization of a silent gene near the INM [15]. We therefore wondered whether the nuclear effectors of the RNAi pathway are required for formation of the specialized nuage domain and/or for the relocalization of the target genes. To explore these possibilities we examined the role of two genes *wago-9/hrde-1* and *nrde-2* required for establishment of heterochromatin at the target locus and for transgenerational inheritance of silencing induced by RNAi. The *wago-9/hrde-1* gene encodes a nuclear Argonaute [16-18], and *nrde-2* encodes a conserved nuclear protein that associates with the target chromatin [14,19]. Neither gene is essential for RNAi when a dsRNA trigger is present, but rather they are only required for transmission of silencing to unexposed offspring. Indeed, *oma-1* dsRNA induced cytological changes in both mutants that resembled in some respects the changes in wild-type animals. For example, cytoplasmic *oma-1* mRNA disappeared, and an enlarged P granule and focus of *oma-1* RNA appeared on each nucleus (compare Figure 2C to Figure 2E and 2G). However in contrast to wild-type worms, germ nuclei in both mutants exhibited two nuclear dots of *oma-1* DNA even at the 21 hr time point, and the dots did not relocalize toward the INM. Moreover, by 21 hours the enlarged P granule had disappeared in both mutants, and lower, equivalent levels of *oma-1* RNA were observed in several P granules (compare

Figure 2D to 2F and 2H). These findings suggest that nuage specialization precedes the activities of WAGO-9 and NRDE-2 in the nuclear RNAi pathway to direct gene relocalization and inherited silencing. The finding that multiple nuage domains ultimately accumulate RNA signal at later times in the nuclear-silencing mutants, suggests that stable differentiation of the specialized nuage domain on the nuclear perimeter requires DNA relocalization.

The above findings indicate that dsRNA-induced transgenerational silencing involves the co-localization of target gene loci to a position on the INM directly adjacent a specialized perinuclear P granule where the corresponding target RNA accumulates. Because the *C. elegans* germline expresses tens of thousands of piRNAs that engage Piwi Argonautes to direct transgenerational silencing of transposons and endongenous genes [4], we wondered if piRNA silencing might also direct a co-localization of target loci and a specialized P granule.

To address this possibility we examined the dosage compensation gene *xol-1*, which is a natural target of piRNA silencing [20]. *xol-1* is repressed in the adult germline of wild-type hermaphrodites, but is de-repressed by mutations in the Piwi Argonaute, *prg-1*. We first examined the XOL-1 (ON) state in *prg-1* mutants to determine where *xol-1* is expressed. Late pachytene nuclei in *prg-1* mutants had *xol-1* DNA and RNA signals similar to the signals seen for *oma-1* in wild-type nuclei without dsRNA. For example, *xol-1* mRNA was detected at low levels in the cytoplasm (Figure 3A late pachytene), and in several perinuclear P granules (Figure 3B), and there were two dots *of xol-1* DNA signal that were not localized by the INM (Figure 3A and B, late). Thus,

153 expression in the XOL-1(ON) state, in the absence of the piRNA pathway, closely
154 resembles expression of an actively transcribed gene, *oma-1*, in wild-type nuclei.

155 To examine the repressed, XOL-1 (OFF) state, we next stained wild-type gonads
156 with a functional piRNA pathway. We found that wild-type gonads lacked detectable *xol-*
157 *1* RNA signal until late pachytene at which time there was a single focus of perinuclear
158 *xol-1* RNA that was coincident with one P granule. DNA FISH revealed that the *xol-1*
159 genes were localized to a single dot coincident with the nuclear RNA signal, and that
160 these signals were by the INM and immediately adjacent to the unique P granule with
161 xol-1 RNA.

162 Although the piRNA-mediated regulation of *xol-1* in late pachytene germ cells
163 closely mirrors the cytological state induced on *oma-1* after 21 hours of RNAi, our
164 results suggest an additional, or different role for PRG-1 in early pachytene germ cells.
165 Examination of *xol-1* RNA and DNA FISH signals during this earlier interval suggests
166 that *prg-1* functions here to prevent the expression of a *xol-1* nuclear RNA. In the *prg-1*
167 mutant this nuclear *xol-1* RNA signal accumulates in proximity to the paired loci at the
168 INM but fails to export or accumulate detectably in the adjacent P granule (compare
169 early pachytene in Figures 3A/B to Figures 3C/D). These findings suggest that in the
170 absence of the piRNA pathway the *xol-1* genes begin transcribing many hours before
171 they separate from the INM and begin to export mRNA. Whether this delay is a
172 peculiarity of the *xol-1* locus or reflects more generally on piRNA regulation will require
173 further study. Taken together, these results suggest that in wild-type animals the piRNA
174 pathway prevents *xol-1* expression entirely in the early pachytene region, and when *xol-*
175 *1* RNA expression commences in late pachytene, PRG-1 and piRNAs promote

accumulation of *xol-1* RNA in an adjacent P granule and the retention of the *xol-1* alleles in proximity to the INM beneath this specialized P granule.

Our results support a model in which transcriptome surveillance by Argonaute pathways is subdivided between specialized perinuclear nuage domains in the *C. elegans* germline (Figure 4). After the initiation of silencing either by piRNAs or dsRNA, cytoplasmic mRNA is rapidly cleared by cytoplasmic Argonautes including WAGO-1, -4, and -7 (yellow Argonautes in the model). By 6 hours, RNA signal becomes limited to a single distinct domain of nuage (a P granule), which expands to accommodate the captured mRNA and to coordinate the programming of the nuclear silencing machinery. Once loaded with these amplified small RNAs, nuclear Argonautes including WAGO-9/HRDE-1 (blue Argonaute in the model) along with other components of the nuclear RNAi pathway (including NRDE-2) help to initiate heterochromatin formation and co-transcriptional silencing. Interestingly, during RNAi the formation of an enlarged domain of nuage precedes and is independent of the nuclear silencing events, and thus appears to recruit or capture the target genes at the nuclear periphery directly adjacent the enlarged P granule.

After the target genes spatially connect to nuage, the nuage diminishes in size, perhaps reflecting the reduced transcriptional activity of the target locus. Indeed, when the nuclear RNAi machinery is disarmed by mutation (Model lower panel), a single enlarged focus of nuage forms during the first 6 hours of exposure to dsRNA, but the target genes ultimately fail to relocalize to the nuclear periphery and mRNA begins to accumulate in multiple additional P granules. Thus our results suggest that the transcriptional silencing machinery participates in a feedback loop that redirects the

target loci and mRNA export to a single domain of nuage. The continued low level transcription of the paired loci at the INM during pachytene may serve to supply template RNA to amplify within the adjacent nuage a small RNA signal that is then transmitted to offspring to propogate silencing.

Thousands of *C. elegans* germline mRNAs are targeted by nearly 1-million distinct Argonaute guide complexes. How the system can simultaneously utilize this many Argonautes to surveil gene expression has been entirely mysterious. Our findings suggest a partial answer to this mystery. Approximately 20 to 50 P granules surround each pachytene nucleus. Therefore, if each P granule is specialized to handle a subset of the RNA silencing load, then each granule need only harbor 50- to 20-thousand guide complexes. Moreover by co-localizing target genes adjacent to nuage domains that maintain their silencing, each P granule need only amplify small RNAs from 40 to 100 different genes in order to service the approximately 2000 protein coding genes that are silenced by the system transgenerationally.

Our findings suggest that each P granule is initially seeded with or differentiates to contain distinct RNA information, and that they utilize this information to guide the transgenerational regulation of their target genes. During oogenesis pachytene P granules dissociate from germ nuclei and flow into the core cytoplasm. P granules from multiple nuclei are captured along with cytoplasm within each maturing oocyte [21]. P granules have liquid-like properties [22]and in the early embryos maternally derived P granules dissolve and reform in early germline blastomeres [23]. These embryonic P granules co-localize with parentally derived Argonaute guide complexes [24,25]. Mutations that disrupt embryonic P granules impair transgenerational inheritance of Argonaute

222 silencing signals [26,27]. Thus it seems likely that when gene expression initiates in the
223 zygotic germline, inherited silencing signals in these embryonic P granules guide the
224 relocalization of germline chromatin to initiate a new round of guide RNA biogenesis
225 and nuage differentiation. If future technical advances permit the direct detection of
226 small RNA species in individual embryonic P granules, it will be interesting to examine
227 whether Argonaute-guide complexes targeting a single gene, for example *xol-1*, or
228 discrete groups of genes, for example those that were served by one pachytene P
229 granule, remain together or whether they become shuffled during the dynamics of early
230 embryogenesis. Whether similar seeds of information form and migrate within and
231 between somatic cells or move from the soma to the germline, and how nuage-like
232 particles compartmentalize and transmit information, and how they orchestrate DNA
233 relocalization, will all require further study. The image of nuage that emerges from these
234 studies mirrors Darwin's notion of gemmules as the units of heredity [28,29]—seeds of
235 parental information that accumulate in germ cells to guide inheritance.

236

237 **Acknowledgements:** We thank Susan Strome from UC Santa Cruz MCD Biology and
238 Karen Bennett from Univerisity of Missouri, School of Medicine for kindly gifting
239 reagents, Christina Baer from SCOPE at UMMS for support with the micromanager
240 installation. We thank Darryl Conte, and members of the Mello and Grunwald labs for
241 help with preparation of the manuscript. This work was supported by a Howard Hughes
242 Medical Institute Investigatorship and NIH R37GM058800 (C.C.M), NSF grant 1614940
243 (D.G.), and NIH RO1GM098583 (J.R.P). . Some of the strains used in this work were

provided by the Caenorhabditis Genetic Center, which is funded by the NIH National Center for Research Resources (NCRR).

Methods:

Worm culture:

The wild-type strain N2 was used and nematodes were cultured as described in[30]. The following transgenic strains were used: **JJ2101**: *zuIs242;* [*nmy-2p*::*PGL-1*::*GFP* + *unc-119(+)*] [6] ZYG-12:GFP **JJ2212**: [*nmy-2p*::*PGL-1*::*mRFP*]. **WH223**: *ojIs*9; [*ZYG-12*::*GFP* + *unc-119(+)*] [11] and WM455, gfp::flag::*xol-1* (ne4555) [20].

Sample preperation for combined FISH, GFP detection and Immunofluorescence

General techniques for gonad dissections were used as described [31]. Briefly, worms were rinsed free of bacteria, then collected in PBS containing 0.1 mM tertramisole (SIGMA L9756) as a paralytic. Once the worms stopped moving, they were placed in PBS for dissection. In some preparations, 0.1% Tween-20 was used to facilitate gonad transfer by micropipette. The dissected gonads were suspended briefly in buffer A (75 mM Hepes (pH 6.9), 40 mM NaCL, 5 mM KCL, 2 mM MgCL2, 1 mM EGTA; all chemicals from Sigma), to which was added a equal volume of fixative buffer B was added (5% paraformaldehyde, 7.5 mM Hepes (pH 7.2), 12 mM NaCL, 1.0 mM KCL, 0.6 mM MgCL2, 0.3 mM EGTA; all chemicals from Sigma). After fixing for 15 mins, the gonads were rinsed, then incubated in RNase-free PBS (ThermoFisher AM9624) containing 0.1% Triton-X100 (Sigma) for 10 mins.The gonads were transferred to room

267 temperature MeOH for 10 mins, then placed in fixative buffer B for an additional 5 mins
268 and rinsed in PBS. Gonads were then dehydrated and stored in EtOH.

269 **RNA and DNA FISH**

270 Gonads stored in EtOH were rehydrated in an EtOH/PBS series, then rinsed and
271 incubated in two changes of wash buffer C (10% formamide, 2XSSC [0.3M NaCL, 30
272 mM sodium citrate (7.0)], 5 mins each. Then the sample was incubated in wash buffer C
273 5°C for 1-3 min, 70° for 3 min, and 60°C for 10-20 min.

274 The wash buffer was replaced with a solution containing ~0.01µM oligo probes
275 (RNA and primary DNA probes), 90% RNA FISH hybridization buffer (Stellarisi SMF-
276 HB-1), and 10% formamide, and incubated at 37ºC overnight in the dark. The samples
277 were rinsed and incubated in wash buffer C for 10 mins at room temperature, then
278 incubated in additional wash buffer at 37ºC for 1 hr. The wash buffer was removed and
279 replaced for a second incubation in wash buffer at 37ºC for 1 hr. For RNA FISH
280 experiments, the gonads were rinsed and held in PBS for immunostaining. For
281 combined RNA and DNA FISH experiments, the gonads were treated with an additional
282 solution containing 0.01 µM Bridge oligo, 0.01µM detection oligo in 2XSSC, 30%
283 formamide at room temperature for 3 hrs. Gonads were washed in prewarmed 2XSSC
284 at 60ºC for 20 min, followed by two washes in 2XSSCT (2XSSC with 0.3% Triton X-100)
285 at 60ºC for 5 min each, and a wash in 2XSSCT at 60ºC for 20 min. Samples were then
286 rinsed at room temperature in 2XSSC. The gonads were rinsed and held in PBS.

287 **Immunostaining**

288 After the FISH protocol was complete gonads in PBS were incubated with primary
289 antibodies diluted in PBS and 0.5 units/µl of RNasin (Promega N261A) at 4ºC overnight.

The antibody solution was removed and the slides rinsed in three changes of PBS, 5 min each. The gonads were then incubated in secondary antibodies diluted in PBS and 0.5 units/µl of RNasin at room temperature for 2 hours. The gonads were rinsed briefly in PBS, then immersed in mounting medium with DAPI (Vectashield H-2000) for imaging. The following antibodies were used: Rabbit anti-PGL-1, a gift from Susan Strome, [32] Chicken anti-GLH-2, a gift from Karen Bennett [33].

Microscope settings and configuration:

All images were acquired on a Yokogawa CSU21 spinning disk confocal microscope mounted onto an Axiovert 200M using a 63x Planapo oil immersion objective with 1.4 N.A. and Zeiss immersion oil. The spinning disk unit add roughly a 2.5 x magnification factor resulting in a pixel size of ~100 nm in the image plane. Images were acquired with a Hamamatsu ImageEM (model c9100-13) series camera using an EM gain of 300. Light from four lasers in a custom laser module (made by Solamere) containing 405 nm, 488 nm, 561 nm and 640 nm laser lines was coupled into a monomode optical fiber and delivered to the Yokogawa scan head. The following bandpass filters (Chroma) were used as emission filters ET-460-50, ET-525-50, ET-605-52, ET-700-75. The sample was mounted using a slide holder and motorized stage (ASI). The microscope was operated using Micromanager[34] software .The integration time per frame was set to 500 ms per frame, except for imaging of the P granula marker GFP::GLH-1 for which the integration time was 400 ms. The camera was set to free read mode. Laser power was adjusted for each sample such as to provide enough signal while keeping bleaching of the sample at bay. The step width between planes along the optical axis was set to 500 nm.

Image processing:

All images were stitched from 9 sub-images that have 50% overlapping with adjacent image [35], but subregions were cropped to size to show desired features in the final figure. Spatial offsets between color channels in lateral (x,y) and axial (z) directions were estimated form bead image stacks using 500 nm sized four color-stained beads (Tetraspecks, Thermo Fisher, Catalog number T14792). The center plane is defined as the plane with the largest diameter signal within a bead and was determined manually in an unprocessed bead image stack. Raw image stacks, after axial offset correction, were filtered using a Gaussian kernel with a width $\sigma = 1$, a Laplacian of Gaussian (LoG3D filter [36]) followed by a Gaussian kernel with a width $\sigma = 1$. The sigma for the LoG3D is chosen for each channel in full pixel values such as to maintain what appears to be the typical spot size for the channel. LoG3D is used for background suppression and not to localize the exact position of a spot. The sigma along the optical axis is taken as roughly half the number of slices the signal is visible in. This approach preserves the visual impression of signal dimension between the channels. The sigma for each channel used was: Ch1: $\sigma_{x,y} = 1$ pixel, $\sigma_z = 2$ pixel; Ch2: $\sigma_{x,y} = 1$pixel, $\sigma_z = 2$ pixel; Ch3: $\sigma_{x,y} = 1$ pixel, $\sigma_z = 2$ pixel.

Figure legends:

Figure 1. (A-L) Merged confocal images of RNA, DNA and Protein signals (as indicated) within the adult hermaphrodite pachytene germline during a time course of *oma-1(RNAi)*. Each larger image shows a projection of ~30 z-layers extending through the entire thickness of the cylindrical gonad. Three smaller insets beneath each projection show enlarged single z-sections through individual nuclei. The coincidence of DNA (green) and RNA (magenta) in (A and C) results in a white signal visible in both the larger multiple z layer projections and in each z-section inset. Similarly, coincidence of P granule (green) and RNA (magenta) signals appear as white in (J, K and L). The scale bar is shown in A. Each of the three horizontal rows corresponds to a time point as indicated at the left (0, 6 and 21 hr). In each row the left pair of images show a gonad stained to detect RNA, DNA and the Nuclear Envelope protein (ZYG-12) and the right pair show a separate gonad stained for RNA DNA and the P granule protein (GFP::GLH-1).

Figure 2. (A-H) Merged confocal images, as in Figure 1, of *oma-1(RNAi)* in wild-type (wt) worms or RNAi pathway mutants at 6-hr and 21-hr time points (as indicated). Each larger image show Z-projections of merged RNA (magenta) and DNA (green) signals within the mid-pachytene region of adult hermaphrodite gonads. The insets show merged RNA (magenta) and P granule (green) signals in individual z-sections. The coincidence of signal is white. P granules were detected using a mixture of sera specific for GLH-2 and PGL-1.

Figure 3. (A-D) Merged confocal images as in Figures 1 and 2 showing wt and *prg-1* mutants (as indicated) expressing the endogenous piRNA-regulated *xol-1* gene fused to *gfp.* DNA and RNA FISH signals were detected with *gfp* specific probes. P granules were detected as described in Figure 2. The insets show individual z-sections and coincident signals are white.

Figure 4. Model

References:

1 Watanabe, T. & Lin, H. Posttranscriptional regulation of gene expression by Piwi proteins and piRNAs. *Mol Cell* **56**, 18-27, doi:10.1016/j.molcel.2014.09.012 (2014).
2 Holoch, D. & Moazed, D. RNA-mediated epigenetic regulation of gene expression. *Nat Rev Genet* **16**, 71-84, doi:10.1038/nrg3863 (2015).
3 Updike, D. & Strome, S. P granule assembly and function in Caenorhabditis elegans germ cells. *J Androl* **31**, 53-60, doi:10.2164/jandrol.109.008292 (2010).
4 Billi, A. C., Fischer, S. E. & Kim, J. K. Endogenous RNAi pathways in C. elegans. *WormBook*, 1-49, doi:10.1895/wormbook.1.170.1 (2014).
5 Pitt, J. N., Schisa, J. A. & Priess, J. R. P granules in the germ cells of Caenorhabditis elegans adults are associated with clusters of nuclear pores and contain RNA. *Dev Biol* **219**, 315-333, doi:10.1006/dbio.2000.9607 (2000).
6 Sheth, U., Pitt, J., Dennis, S. & Priess, J. R. Perinuclear P granules are the principal sites of mRNA export in adult C. elegans germ cells. *Development* **137**, 1305-1314, doi:10.1242/dev.044255 (2010).
7 Fire, A. *et al.* Potent and specific genetic interference by double-stranded RNA in Caenorhabditis elegans. *Nature* **391**, 806-811, doi:10.1038/35888 (1998).
8 Ji, N. & van Oudenaarden, A. Single molecule fluorescent in situ hybridization (smFISH) of C. elegans worms and embryos. *WormBook*, 1-16, doi:10.1895/wormbook.1.153.1 (2012).
9 Fields, B. D., Nguyen, S. C., Nir, G. & Kennedy, S. A multiplexed DNA FISH strategy for assessing genome architecture in Caenorhabditis elegans. *Elife* **8**, doi:10.7554/eLife.42823 (2019).

10 Beliveau, B. J. *et al.* Single-molecule super-resolution imaging of chromosomes and in situ haplotype visualization using Oligopaint FISH probes. *Nat Commun* **6**, 7147, doi:10.1038/ncomms8147 (2015).

11 Malone, C. J. *et al.* The C. elegans hook protein, ZYG-12, mediates the essential attachment between the centrosome and nucleus. *Cell* **115**, 825-836, doi:10.1016/s0092-8674(03)00985-1 (2003).

12 Roussell, D. L. & Bennett, K. L. glh-1, a germ-line putative RNA helicase from Caenorhabditis, has four zinc fingers. *Proc Natl Acad Sci U S A* **90**, 9300-9304, doi:10.1073/pnas.90.20.9300 (1993).

13 Chen, C. C. *et al.* A member of the polymerase beta nucleotidyltransferase superfamily is required for RNA interference in C. elegans. *Curr Biol* **15**, 378-383, doi:10.1016/j.cub.2005.01.009 (2005).

14 Burton, N. O., Burkhart, K. B. & Kennedy, S. Nuclear RNAi maintains heritable gene silencing in Caenorhabditis elegans. *Proc Natl Acad Sci U S A* **108**, 19683-19688, doi:10.1073/pnas.1113310108 (2011).

15 Ahringer, J. & Gasser, S. M. Repressive Chromatin in Caenorhabditis elegans: Establishment, Composition, and Function. *Genetics* **208**, 491-511, doi:10.1534/genetics.117.300386 (2018).

16 Buckley, B. A. *et al.* A nuclear Argonaute promotes multigenerational epigenetic inheritance and germline immortality. *Nature* **489**, 447-451, doi:10.1038/nature11352 (2012).

17 Ashe, A. *et al.* piRNAs can trigger a multigenerational epigenetic memory in the germline of C. elegans. *Cell* **150**, 88-99, doi:10.1016/j.cell.2012.06.018 (2012).

18 Shirayama, M. *et al.* piRNAs initiate an epigenetic memory of nonself RNA in the C. elegans germline. *Cell* **150**, 65-77, doi:10.1016/j.cell.2012.06.015 (2012).

19 Guang, S. *et al.* Small regulatory RNAs inhibit RNA polymerase II during the elongation phase of transcription. *Nature* **465**, 1097-1101, doi:10.1038/nature09095 (2010).

20 Tang, W. *et al.* A Sex Chromosome piRNA Promotes Robust Dosage Compensation and Sex Determination in C. elegans. *Dev Cell* **44**, 762-770 e763, doi:10.1016/j.devcel.2018.01.025 (2018).

21 Wolke, U., Jezuit, E. A. & Priess, J. R. Actin-dependent cytoplasmic streaming in C. elegans oogenesis. *Development* **134**, 2227-2236, doi:10.1242/dev.004952 (2007).

22 Brangwynne, C. P. *et al.* Germline P granules are liquid droplets that localize by controlled dissolution/condensation. *Science* **324**, 1729-1732, doi:10.1126/science.1172046 (2009).

23 Seydoux, G. The P Granules of C. elegans: A Genetic Model for the Study of RNA-Protein Condensates. *J Mol Biol* **430**, 4702-4710, doi:10.1016/j.jmb.2018.08.007 (2018).

24 Claycomb, J. M. *et al.* The Argonaute CSR-1 and its 22G-RNA cofactors are required for holocentric chromosome segregation. *Cell* **139**, 123-134, doi:10.1016/j.cell.2009.09.014 (2009).

25 Gu, W. *et al.* Distinct argonaute-mediated 22G-RNA pathways direct genome surveillance in the C. elegans germline. *Mol Cell* **36**, 231-244, doi:10.1016/j.molcel.2009.09.020 (2009).

26 Dodson, A. E. & Kennedy, S. Germ Granules Coordinate RNA-Based Epigenetic Inheritance Pathways. *Dev Cell* **50**, 704-715 e704, doi:10.1016/j.devcel.2019.07.025 (2019).

27 Ouyang, J. P. T. *et al.* P Granules Protect RNA Interference Genes from Silencing by piRNAs. *Dev Cell* **50**, 716-728 e716, doi:10.1016/j.devcel.2019.07.026 (2019).

28 Choi, Y. & Mango, S. E. Hunting for Darwin's gemmules and Lamarck's fluid: transgenerational signaling and histone methylation. *Biochim Biophys Acta* **1839**, 1440-1453, doi:10.1016/j.bbagrm.2014.05.011 (2014).

29 Liu, Y. In Search of Darwin's Imaginary Gemmules. *Adv Genet* **101**, 87-114, doi:10.1016/bs.adgen.2018.05.004 (2018).

30 Brenner, S. The genetics of Caenorhabditis elegans. *Genetics* **77**, 71-94 (1974).

31 Raiders, S. A., Eastwood, M. D., Bacher, M. & Priess, J. R. Binucleate germ cells in Caenorhabditis elegans are removed by physiological apoptosis. *PLoS Genet* **14**, e1007417, doi:10.1371/journal.pgen.1007417 (2018).

32 Kawasaki, I. *et al.* PGL-1, a predicted RNA-binding component of germ granules, is essential for fertility in C. elegans. *Cell* **94**, 635-645, doi:10.1016/s0092-8674(00)81605-0 (1998).

33 Gruidl, M. E. *et al.* Multiple potential germ-line helicases are components of the germ-line-specific P granules of Caenorhabditis elegans. *Proc Natl Acad Sci U S A* **93**, 13837-13842, doi:10.1073/pnas.93.24.13837 (1996).

34 Edelstein, A., Amodaj, N., Hoover, K., Vale, R. & Stuurman, N. Computer control of microscopes using microManager. *Curr Protoc Mol Biol* **Chapter 14**, Unit14 20, doi:10.1002/0471142727.mb1420s92 (2010).

35 Preibisch, S., Saalfeld, S. & Tomancak, P. Globally optimal stitching of tiled 3D microscopic image acquisitions. *Bioinformatics* **25**, 1463-1465, doi:10.1093/bioinformatics/btp184 (2009).

36 Sage, D., Neumann, F. R., Hediger, F., Gasser, S. M. & Unser, M. Automatic tracking of individual fluorescence particles: application to the study of chromosome dynamics. *IEEE Trans Image Process* **14**, 1372-1383, doi:10.1109/tip.2005.852787 (2005).

Figure 1

https://doi.org/10.1101/2021.03.09.434681

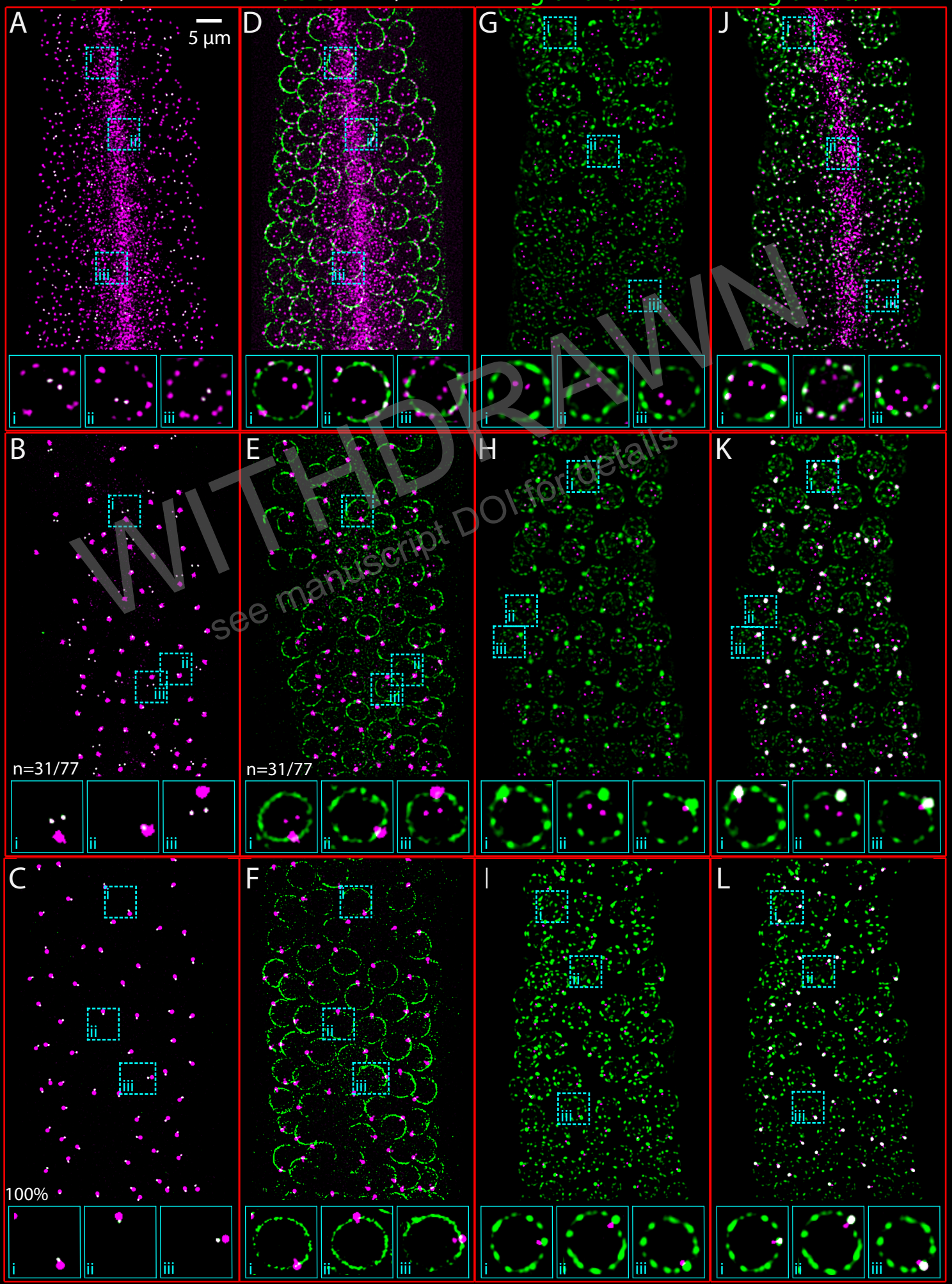

Figure 2

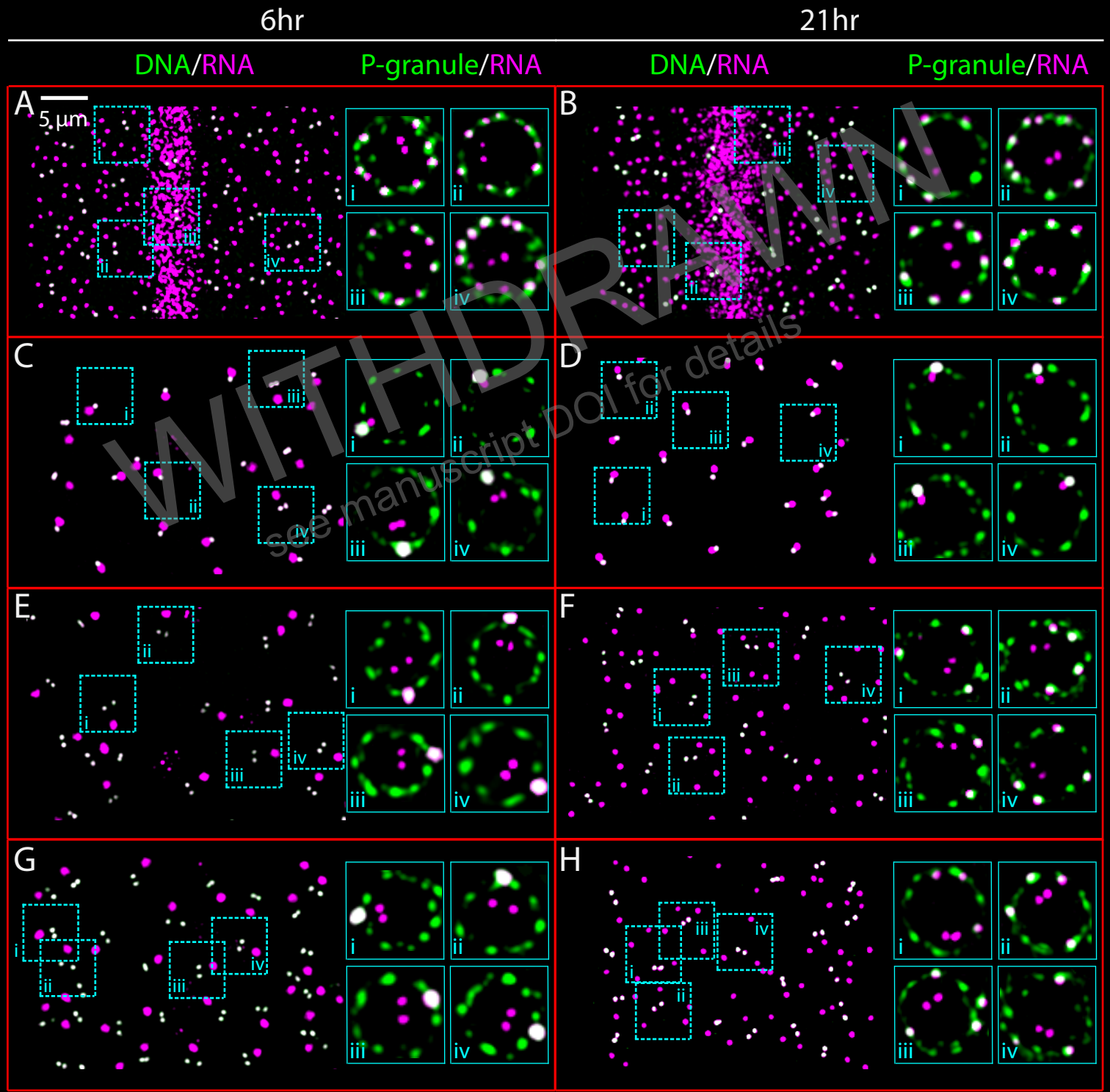

Figure 3

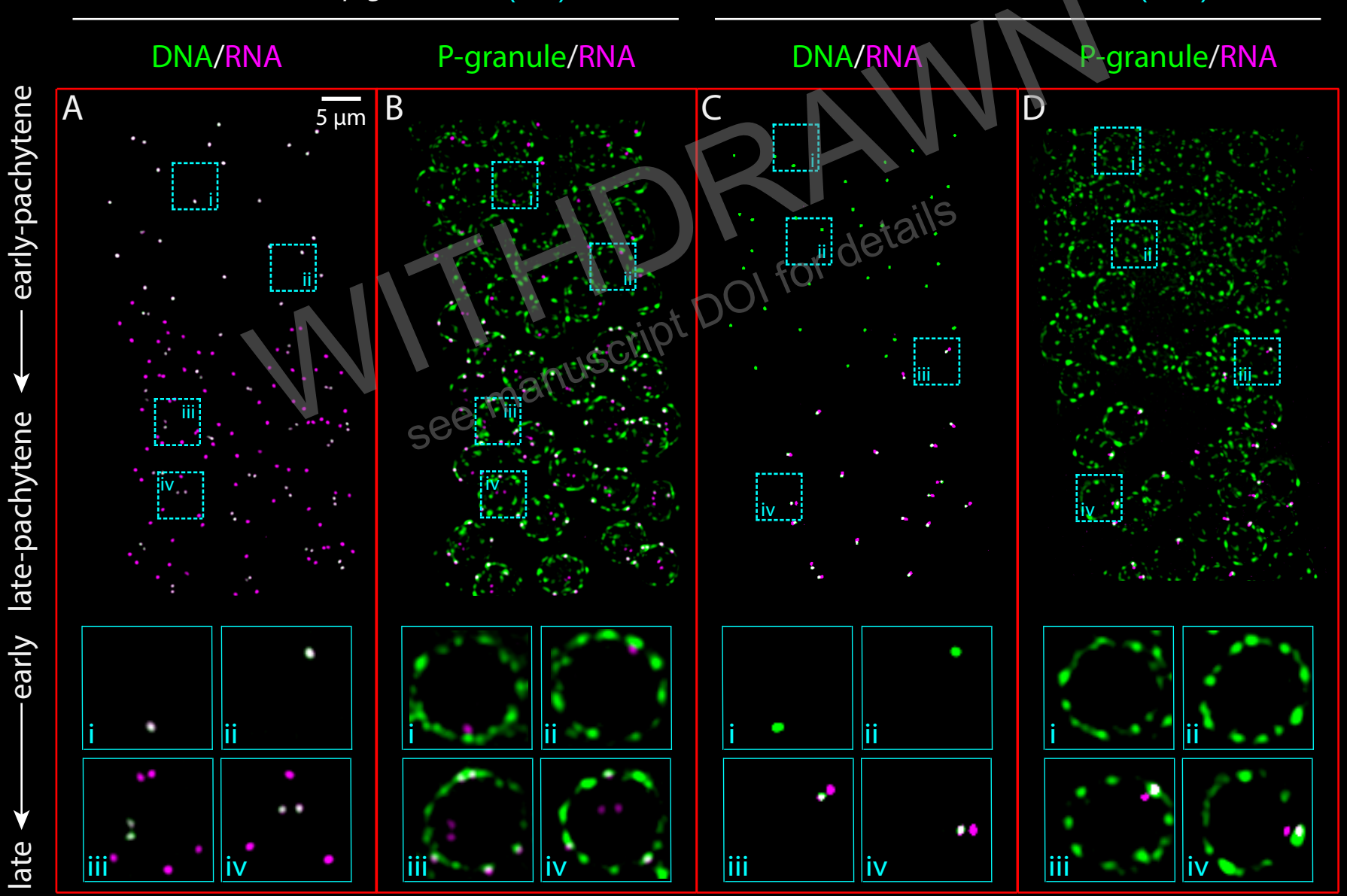

Figure 4 Model

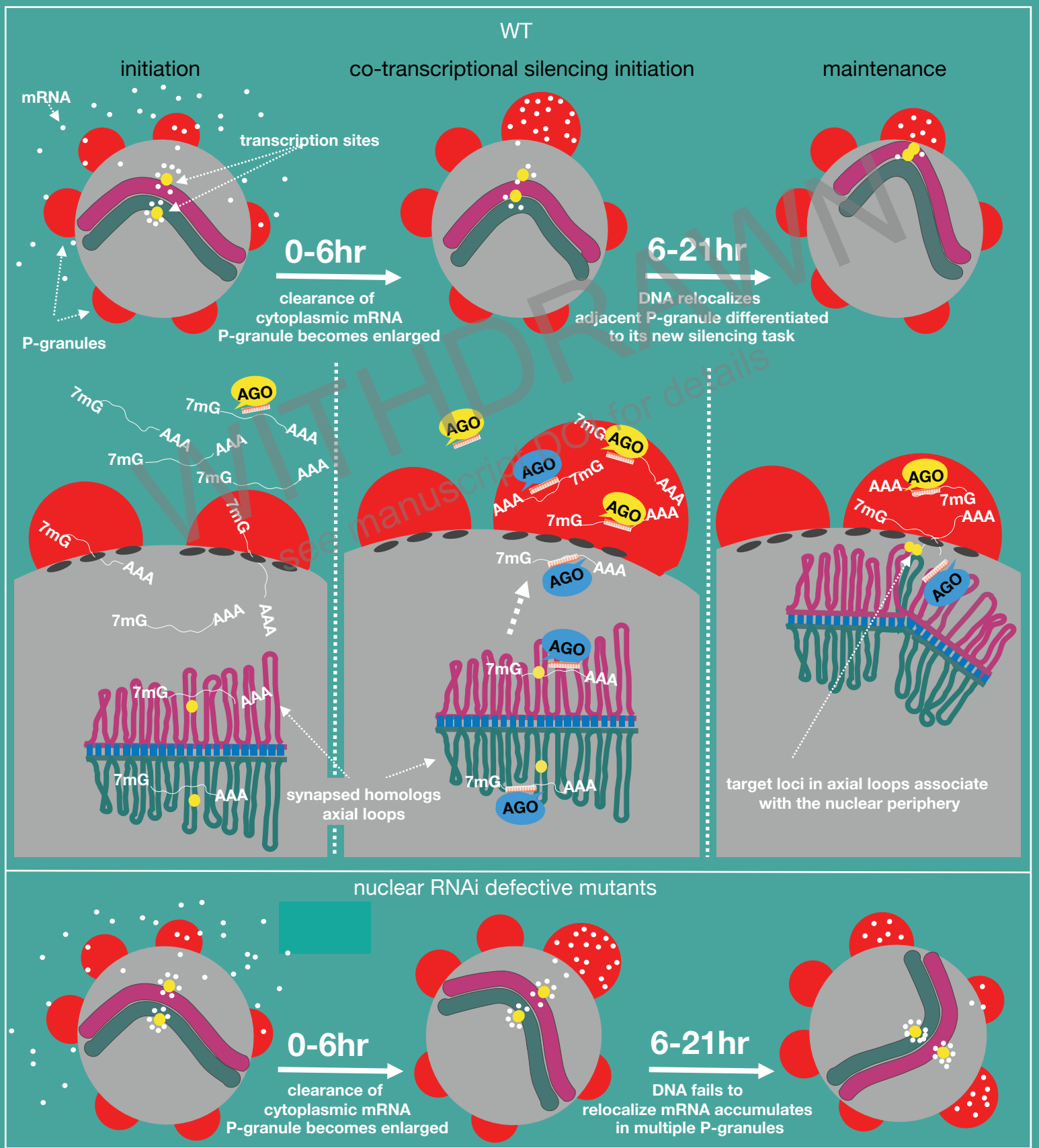

Sup Figure 2